

Hexagons are the Bestagons: Design Automation for Silicon Dangling Bond Logic

Marcel Walter
Technical University of Munich
Chair for Design Automation
Munich, Bavaria, Germany
marcel.walter@tum.de

Konrad Walus
University of British Columbia
Department of Electrical and Computer Engineering
Vancouver, British Columbia, Canada
konradw@ece.ubc.ca

Samuel Sze Hang Ng
University of British Columbia
Department of Electrical and Computer Engineering
Vancouver, British Columbia, Canada
samueln@ece.ubc.ca

Robert Wille
Chair for Design Automation, Technical University of
Munich, Germany
Software Competence Center Hagenberg GmbH, Austria
robert.wille@tum.de

ABSTRACT

Field-coupled Nanocomputing (FCN) defines a class of post-CMOS nanotechnologies that promises compact layouts, low power operation, and high clock rates. Recent breakthroughs in the fabrication of *Silicon Dangling Bonds* (SiDBs) acting as quantum dots enabled the demonstration of a sub-30 nm² OR gate and wire segments. This motivated the research community to invest manual labor in the design of additional gates and whole circuits which, however, is currently severely limited by scalability issues. In this work, these limitations are overcome by the introduction of a design automation framework that establishes a flexible topology based on hexagons as well as a corresponding *Bestagon* gate library for this technology and, additionally, provides automatic methods for physical design. By this, the first design automation solution for the promising SiDB platform is proposed. In an effort to support open research and open data, the resulting framework as well as all design and code files are made publicly available.

CCS CONCEPTS

• **Hardware** → **Quantum dots and cellular automata**; **Placement**; **Wire routing**; **Physical synthesis**; **Clock-network synthesis**; *Technology-mapping*; *Combinational synthesis*; Circuit optimization; Design databases for EDA; *Software tools for EDA*; Equivalence checking; **Simulation and emulation**; *Theorem proving and SAT solving*; Design rule checking.

1 INTRODUCTION & MOTIVATION

Post-CMOS *Field-coupled Nanocomputing* (FCN) [2] technologies promise the possibility to realize nanometer-sized elementary logic-in-memory devices [20, 33], offer energy dissipation capabilities below the *Landauer limit* [20–22, 25, 42], or clock frequencies in the terahertz regime [27, 41]. For all these endeavors, FCN serves as an umbrella term for a class of emerging technologies that perform computations via the repulsion of physical fields instead of electrical current flow. Recent years have established tremendous advancements in the fabrication of *Silicon Dangling Bonds* (SiDBs) [1, 15, 18, 19, 31, 53] which exhibit quantum-dot behavior, an application which has been dubbed *atomic silicon quantum dots*. They can be used to implement logic under the FCN paradigm as proven by experimental demonstrations of a sub-30 nm² SiDB OR gate [18]; ushering in an exciting platform at the limit of scaling.

Motivated by the promise of these experimental demonstrations, the research community has started to show great interest in the SiDB platform; with multiple computational explorations leading to

various manually designed gates and circuits [3, 10, 11, 29, 30, 45] along with promises of low-power and high frequency operation in a post-CMOS realm [10, 11, 29]. However, scaling up would greatly benefit from the contributions of the design automation community towards corresponding design frameworks, which do not currently exist for the SiDB platform. This is in contrast to other FCN implementations such as *Quantum-dot Cellular Automata* (QCA) [23] for which methodologies exist that respect the corresponding physical-level design rules [11, 17, 37], utilize established standard cell libraries [36] as well as technology-specific clocking strategies [5, 9, 26, 44], and provide tailored placement and routing algorithms [13, 43, 46, 49].

Unfortunately, those accomplishments cannot directly be used for SiDB since the corresponding physical basics (as demonstrated in [18]) require a substantially different approach. For example, whereas existing FCN design automation frameworks encode logic in terms of rectangular arrangements of quantum dots laid out on a Cartesian grid, this work shows that the SiDB platform is much more suited for a hexagonal architecture. This topology shift has heavy consequences on the correspondingly needed gate library, the resulting design rules, and the way physical design is supposed to be conducted. In this work, those challenges are addressed by

- (1) the establishment of a hexagonal floor plan topology,
- (2) the proposal of the *Bestagon* gate library, i. e., a set of hexagonal standard component tiles, which is carefully attuned to SiDB's technological constraints with validation from the platform-specialized CAD tool *SiQAD* [30],
- (3) a design rule framework that respects current fabrication technology for clocking electrodes, physical limitations of Coulombic bias, and similar constraints, as well as
- (4) a physical design flow that uses the proposed hexagonal floor plans, gate library, and design rules to automatically generate dot-accurate SiDB circuit layouts from logical specifications.

Hence, this paper proposes the first design automation flow for SiDB. The resulting implementation is publicly provided as open source together with all obtained design files at [52].

The remainder of this manuscript is structured as follows: in an effort to establish this paper as a stand-alone work, Section 2 reviews related material on the SiDB logic platform to constitute the foundation upon which this paper is built. Section 3 discusses the challenges for design automation of SiDBs and proposes general ideas of corresponding solutions. Based on that, Section 4 presents the *Bestagon* library of hexagonal standard tiles, physical design rule restrictions as well as a proposal for a physical design flow. In Section 5, an example analysis of hexagonal adaptations of physical

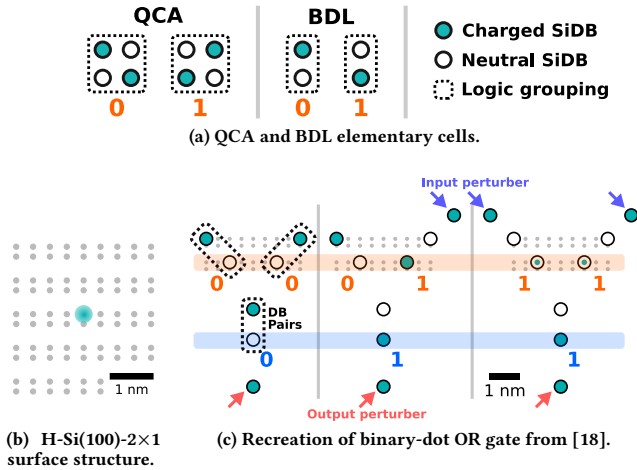


Figure 1: (a) QCA and BDL logic cells showing two forms of FCN implementations. Charged SiDBs are negatively charged in the context of this work. (b) Surface lattice structure of H-Si(100)-2 \times 1 with hydrogen sites depicted in gray and an SiDB depicted in teal halo; removal of hydrogen sites results in SiDBs. (c) BDL OR gate from [18] recreated in *SiQAD* and simulated with *SimAnneal* [30] with $\mu = -0.28$ eV, $\epsilon_r = 5.6$, and $\lambda_{TF} = 5$ nm. Orange and blue shades highlight the logic state of input and output SiDB pairs respectively. Lattice dots are only partially drawn for visual clarity.

design algorithms is conducted and obtained SiDB layouts are discussed. Finally, Section 6 concludes the paper and gives an outlook on future work in the domain.

2 PRELIMINARIES & RELATED WORK

Notable implementations of FCN include charge-coupled [6, 23, 24, 33, 39] and magnetically-coupled [4, 12] devices. The former relies on ensembles of quantum dots—minuscule devices which can hold discrete charge states. A popular implementation is QCA which encode bit information in charge locations in rectangular arrays of quantum dots as illustrated in Figure 1a [23]; in some cases, additional charge sites are used for *null* logic states [24]. An alternative implementation is to encode bit-states in pairs of quantum dots, dubbed *Binary-dot Logic* (BDL) [18], also illustrated in Figure 1a.

Among quantum-dot FCN implementations in the literature, the use of SiDBs on the hydrogen-passivated silicon(100) 2 \times 1 (H-Si(100)-2 \times 1) surface is particularly intriguing as they are able to act as atomically-sized quantum dots [15, 18, 32, 35, 53], placing them at the ultimate limit of scaling. The H-Si(100)-2 \times 1 surface has discretely defined sites where SiDBs can be fabricated with atomic precision using the probe of scanning tunneling microscopes [1, 19, 31], as illustrated in Figure 1b. A groundbreaking demonstration by Huff *et al.* [18] has shown experimentally that careful configurations of SiDBs can be used to construct BDL logic components.

In the demonstrated system setup, SiDBs may possess 0, 1, or 2 electrons, corresponding to positive, neutral, and negative charge states respectively. In simulations throughout this work, SiDBs with cyan fill represent negatively charged sites and hollow SiDBs represent neutral sites; positive charge states are not relevant to the configuration of interest [18, 30]. The charge states can be influenced by

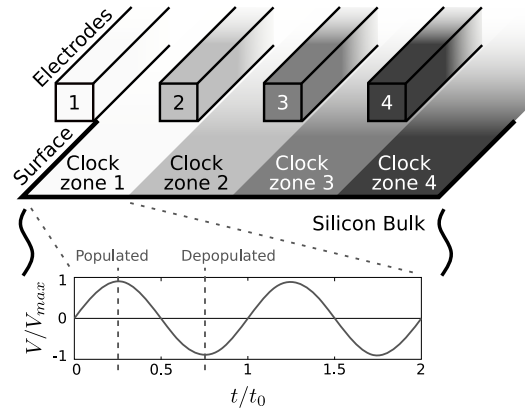


Figure 2: Illustration of clocking by charge population modulation to divide *activated* and *deactivated* circuit regions.

environmental factors such as the bulk dopant concentration [34] and the presence of electric fields [32]. In the absence of deliberate excitations, charges in SiDB systems exhibit a tendency to settle to low-energy configurations at both cryogenic [18, 35] and room temperatures [15]—a behavior that is desirable for charge-based ground state FCN logic.

These electronic properties enable the demonstration of BDL wire structures as well as a sub 30 nm² logic OR gate at the nanoscale [18]. A simulated reproduction of the OR gate is shown in Figure 1c. Here, the input bit state is set by the existence of a peripheral SiDB, dubbed a *perturber* [18, 30], which exerts Coulombic pressure on the input SiDB-pair to emulate the presence of an input BDL wire at logic 1 state. An output perturber is present to emulate the presence of an output BDL wire. It can be observed that when one or both of the input SiDB pairs are set to logic 1 by input perturbers, the output also toggles to logic 1 state as expected of an OR gate. It is to be noted that the need for these perturbers will be alleviated upon the future development of I/O devices.

Prospective scaling of SiDB FCN systems requires the introduction of clocking and I/O circuitry. Hereby, clocking is a necessity for any sufficiently large FCN circuit layout—combinational or sequential. Clocking in FCN stabilizes signals and directs the flow of information in a pipeline-like fashion by alternately expressing certain *activated* regions which are able to hold logic states and carry out computations, and *deactivated* regions which act as separators and reduce cross-talk [16, 26]. SiDB clocking is expected to be achieved through the modulation of surface charge populations where segments can be deactivated by removing surface charges, creating an electrically neutral region [11, 30, 32]. To enforce information flow in designated directions, past SiDB logic research has proposed the use of a prevalent clocking strategy from FCN literature, i. e., four-phase clocking [11, 30], illustrated in Figure 2. For the benefit of design automation and design rule enforcement, there also exist proposals of various tileable clocking floor plans; the most common of them being *Columnar* [26], *2DDWave* [44], and *USE* [9]. As for interfacing between the atomic circuits and macro CMOS circuits, past works proposed the use of near-surface electrodes to set the input logic state of SiDB logic cells [11] and *single-electron transistors* for logic read-out [14, 18, 30].

Recently, the barrier of entry for further exploration into the SiDB platform was lowered by *SiQAD*, a CAD tool that offers SiDB-specific manual design features and calibrated physical simulation engines [11, 30]. A variety of logic gates and circuits have been

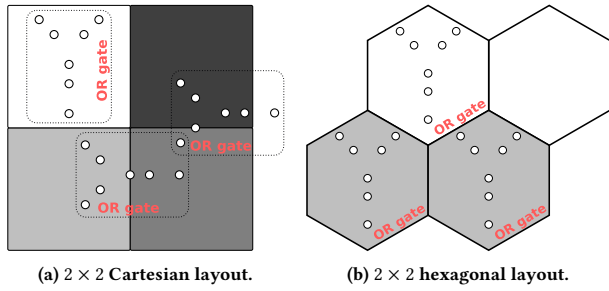


Figure 3: (a) When strictly connecting inputs to outputs, Y-shaped SiDB gates do not fit into the structure of Cartesian grids as elementary building blocks. (b) Hexagonal grids can host Y-shaped SiDB gates without modifications.

proposed and verified via *SiQAD*—including Y-shaped gates similar to Huff *et al.*'s experimental demonstrations [30], T-shaped, plus-shaped, and box-shaped ones, some of which implement 3-input functions [3, 45], as well as QCA-like gates adapted to the SiDB platform [29].

However, despite the above accomplishments, these efforts remain manual and have yet to receive attention from the design automation community. Although lessons can be learned from design approaches for other FCN implementations [5, 13, 17, 36, 43, 46, 48, 49, 51], there still exist domain-specific restrictions and obstacles for SiDBs which are addressed in detail in the following Section 3.

3 DESIGN CHALLENGES & GENERAL IDEAS

This paper aims at establishing the first physically sound design rule framework for SiDBs. To this end, this work heavily considers the experimentally proven implementations by Huff *et al.* [18], existing physical models [10, 30], and realistic fabrication capabilities [1, 54]. However, to realize correspondingly sound designs, the following challenges need to be addressed.

Layout Topology: The OR gate demonstrated by Huff *et al.* and reviewed in Figure 1c is Y-shaped, which is an unusual shape for an FCN gate to have. Since previous FCN gates, especially for QCA, have their inputs and outputs orthogonally aligned due to their plus-shape, Cartesian layout structures were established as tile-based floor plans for physical design algorithms [17]. However, such Cartesian grids cannot reasonably accommodate Y-shaped gates as illustrated in Figure 3a—it can be observed that connections of inputs and outputs cannot properly be fitted into the Cartesian coordinate structure. Thus, established settings and physical design methods for the FCN domain are not suitable for placement & routing of the only experimentally verified SiDB gate type.

Hence, in order to respect the Y-shape gate configuration in the layout generation process, this paper proposes to utilize hexagonal grids instead of Cartesian ones. This hexagonal topology natively matches the demonstrated SiDB gate structure, as shown in Figure 3b. In this orientation, the input pins of all gates are directly accessible via the center of tile borders and the gates' output can be propagated to either of the two bottom directions. Within each hexagonal tile, the gate can naturally be rotated or mirrored. This, however, requires new and correspondingly developed design methods.

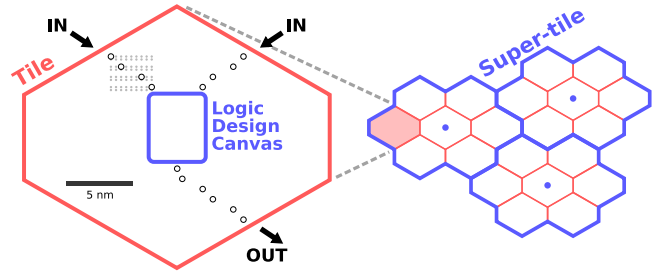


Figure 4: Due to limits imposed by the minimum metal pitch for clocking electrodes, each addressable clock zone may cover multiple standard tiles, dubbed a *super-tile*. Depicted on the left is an example of a 2-in-1-out *Bestagon* tile template containing standard input and output wires and a blank design canvas. On the right is an example of how tiles and super-tiles may be arranged. Tiles are outlined in red, super-tiles in blue with a blue dot indicating their centers.

Extended Gate Library: Huff *et al.*'s experimental demonstration of SiDB logic structures physically validated a Y-shaped OR gate (Figure 1c) and BDL wires [18]. However, logic layout generation requires additional components such as inverters, fan-out wires, and wire crossings. Moreover, standard libraries usually offer a broader variety of gate types to enable more cost-efficient technology-mapped logic networks and layouts.

Hence, in this work, a corresponding gate library—coined the *Bestagon* library—is proposed which is designed with this versatility and flexibility in mind. The proposed gate tiles implement various Boolean functions and resemble the established Y-shaped topology as closely as possible.

Clocking Constraints: With a footprint of merely 30 nm^2 , Huff *et al.*'s OR gate operates at the limit of scaling. This impressive achievement, which aces conventional fabrication, is simultaneously a blessing and a curse. While it theoretically allows for ultra area-efficient designs, current technology nodes cannot offer fabrication for clocking electrodes that match the OR gate's dimensions. This circumstance dictates that realistic clock zone dimensions must be significantly greater than the demonstrated individual gate sizes.

Hence, in order to additionally enable clocked designs, this work proposes to group multiple hexagonal tiles together in regions large enough to be driven by the same clocking electrode. All tiles in each resulting *super-tile* are exposed to the same clock field respectively and, thus, switch simultaneously. Innately, this approach restricts the obtained layouts to specific linear clocking schemes but ensures their physical fabricability.

4 DESIGN AUTOMATION FOR SiDBS

Motivated by the challenges and corresponding ideas proposed in the preceding section, a holistic set of design rules is obtained in the following, which is utilized to create a library of Y-shaped gates on uniform hexagonal standard tiles that respect state-of-the-art fabrication restrictions regarding clocking constraints and physical limitations. Since the hexagonal layout topology, the Y-shaped gate structures, and the clocking constraints are highly interdependent, they are discussed as one interwoven entity in Section 4.1 with the goal to obtain the *Bestagon* gate library that conforms to the discussed constraints. Afterward, Section 4.2 presents a corresponding design flow for the obtainment of dot-accurate SiDB circuit

layouts via the utilization of the *Bestagon* library and adapted logic synthesis and physical design algorithms.

4.1 The Bestagon Gate Library

Section 3 discussed three design challenges and proposed solutions in the process of design automation for SiDBs. This section describes how to holistically address these three points, yielding a set of standard tiles—the *Bestagon* gate library.

The design of these standard tiles is informed by the consideration of realistic physical limitations of the clocking network and requires to keep the proposed logic layouts in line with Huff *et al.*'s demonstrated Y-shaped gates [18]. At state-of-the-art 7 nm lithography processes, the minimum metal pitch is 40 nm [54]. In comparison, Huff *et al.*'s OR gate has dimensions within 5 nm×6 nm, which constitutes two options in designing the tiles: (1) extend the lengths of input and output BDL wires leading to the logic component at the center of the tile such that each tile is large enough to be individually addressable by a clocking electrode without violating the minimum metal pitch, or (2) maintain the ≈ 10 nm dimension for the core component tiles and group multiple of these tiles inside a *super-tile*, a collection of tiles large enough to be addressed as a single unit by a clocking electrode.

The former option offers individually addressable standard tiles at the cost of lower logic density; the latter allows the maintaining of logic density at the expense of potential complications in the handling of detailed information flow within the super-tiles. In this work, it is chosen to explore the latter path of higher logic density with the use of smaller standard tiles while managing the complexity of the placement and routing problem by relying on feed-forward clocking floor plans, e. g., *Columnar* [26] or *2DDWave* [44].

Henceforth, each tile in the proposed *Bestagon* library is of hexagonal shape and consists of input and output BDL wires for connection and a *logic design canvas* in the center for logic implementation. An example of a 2-in-1-out tile template is illustrated in Figure 4. Input and output wire lengths are chosen such that the logic design canvases of adjacent tiles in all directions have at least 10 nm distance in order to reduce direct interference between logic components when using physical parameters calibrated to [18, 30]. For this study, templates for 1-in-1-out, 1-in-2-out, 2-in-1-out, and 2-in-2-out are proposed, including designed tiles for wires (vertical, diagonal, two parallel verticals), wire crossings, fan-outs, single-tile half adders, inverters (straight and diagonal), and common 2-in-1-out gates including OR, AND, NOR, NAND, XOR, and XNOR. Simulation results of select gate designs using the *SimAnneal* ground state finder in *SiQAD* are shown in Figure 5, with the rest available in an open repository [52].

These tiles have been designed with the assistance of a reinforcement learning agent [28] which is allowed to place SiDBs within the logic design canvas and toggle through input combinations to check for logic correctness. The layouts are manually reviewed and edited as needed for inclusion in the library.

The toggling of input logic states to the component tiles is a refinement upon Huff *et al.*'s methodology [18]: whereas Huff *et al.* represent a logic 1 input by the existence of an input perturber and logic 0 by the lack of it (see Figure 1c), this work employs the input perturber for both logic 0 and 1 states but created at either farther or closer locations, respectively. This constitutes a more realistic representation of the repulsion exerted by upstream input logic wires because at logic 0, Huff *et al.*'s method of removing the perturber does not capture any upstream input influence whereas the proposed method does. Ultimately, this approach generates gates that are more robust to disturbances of nearby SiDB structures.

The obtained *Bestagon* tiles are used in later sections for placement and routing demonstrations. Figure 6 shows such an employment of the tiles in a placed and routed implementation of the *par_check* benchmark from [43] (design flow detailed in the subsequent section). Logic signals flow from the top to bottom due to the employment of the *Columnar* clocking scheme [26] rotated by 90° yielding a row-based configuration where tile (x, y) is driven by clock zone $y \bmod 4$.

The depicted layout incorporates six different logic gates from the *Bestagon* library plus two wire configurations, fan-outs, and a crossing, which makes it a prime representative for the benefits of the proposed methods; namely ultra-dense physically sound and fabricable logic structures with a high Boolean expressiveness due to a variety of tile-based components.

4.2 Resulting Physical Design Flow

With the definition of the *Bestagon* gate library that complies with the hexagonal topology for Y-shaped gates and clocking constraints imposed by physical and fabrication limitations, certain established design automation principles from the QCA domain can be accordingly adjusted. This eventually results in a design flow that uses the *Bestagon* library and complies with the discussed design rules. The flow starts with specifications at the logic level, e. g., provided by gate-level Verilog or similar files, and automatically generates dot-accurate SiDBs layouts that implement the given functions and can be processed further by simulators, e. g., *SiQAD* [30] or for physical realization/fabrication.

The proposed flow is as follows:

- (1) parse a specification file as *XOR-AND-Inverter Graph* (XAG),
- (2) perform cut-based logic rewriting with an exact NPN database to reduce the XAG's size and depth [38],
- (3) perform technology mapping [8] to restructure XAG nodes into gates supported by the proposed *Bestagon* library,
- (4) generate a linearly clocked hexagonal gate-level layout from the mapped network via SMT-based *exact* [46] physical design,
- (5) perform SAT-based equivalence checking of the input network and the resulting gate-level layout [50],
- (6) merge adjacent tiles into super-tiles by expanding the clock zone dimensions,
- (7) apply the *Bestagon* library to map each gate to a dot-accurate representation yielding an SiDB layout, and
- (8) generate a design file from the SiDB layout for physical simulation and/or fabrication.

Since the *Bestagon* gate library supports both AND and XOR standard tiles, XAGs have been picked as the data structure of choice for the logic synthesis part as they offer a potentially more compact representation compared to *AND-Inverter-Graphs* (AIGs) with only a slight overhead in memory consumption.¹ The optimized XAGs then serve as input to the physical design algorithm from [46] which—via some adjustments—is able to support both hexagonal layout topologies and the *Bestagon* library. However, since the algorithm does not support super-tiles, the additional step of clock zone expansion becomes necessary.

In order to validate the integrity and verify the logical correctness of the resulting layouts, SAT-based equivalence checking as proposed in [50] is applied first followed by physical simulation with *SiQAD* to ascertain operational behavior under known physical models.

¹Even though there exist even more expressive data structures, e. g., *XOR-Majority-Inverter-Graphs* (XMGs), they usually represent logic by the means of Boolean functions that are unsupported by the *Bestagon* gate library, e. g., Majority.

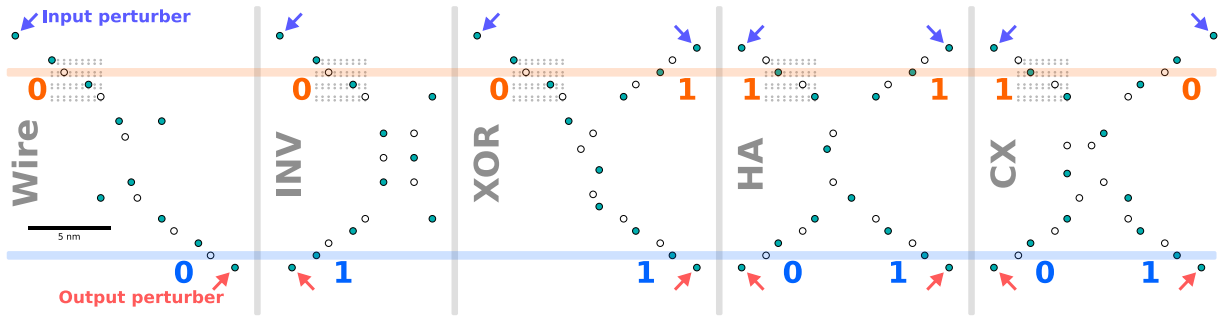


Figure 5: Simulation results of select *Bestagon* logic gates via *SimAnneal* [30] with $\mu_- = -0.32$ eV, $\epsilon_r = 5.6$, $\lambda_{TF} = 5$ nm.

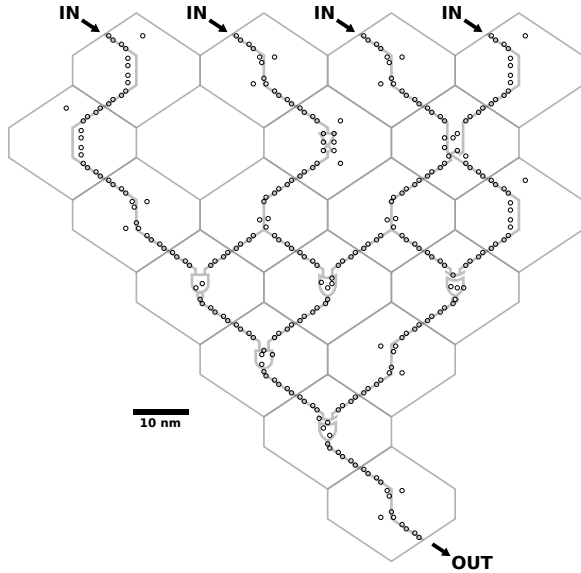


Figure 6: Synthesized layout of SiDB *Bestagon* gates on hexagonal tiles implementing the *par_check* benchmark from [43] with an underlaid circuit diagram hinting at the tile functions. SiDBs are depicted as circles (which are not to scale for better visibility). Information flows from top to bottom in the layout and logic correctness is ensured via formal verification.

In order to implement this flow, any algorithms for logic optimization, technology mapping, physical design, and formal verification can be applied as long as they are adjusted to respect the design rules proposed in this paper. Consequentially, it is also possible to create a variety of gate libraries following the provided specifications to cover a larger part of the Boolean domain with elementary building blocks.

Therefore, a corresponding design automation framework was implemented that precisely follows the flow outlined above. It is confirmed in the following section that said implementation is in fact applicable for the generation of logically correct and physically feasible dot-accurate SiDB layouts.

5 APPLICATION

Whereas the previous sections provided a detailed description of the obtainment and specifics of the *Bestagon* library in accordance with

Table 1: Excerpt of generated layout data

Name	$w \times h = A$	SiDBs	nm^2
xor2	$2 \times 3 = 6$	58	2 403.98
xnor2	$2 \times 3 = 6$	58	2 403.98
[43] par_gen	$3 \times 4 = 12$	103	4 830.22
mux21	$3 \times 6 = 18$	196	7 258.52
par_check	$4 \times 7 = 28$	284	11 312.68
xor5_r1	$5 \times 6 = 30$	232	12 124.57
xor5_majority	$5 \times 6 = 30$	244	12 124.57
t	$5 \times 8 = 40$	426	16 180.79
t_5	$5 \times 8 = 40$	448	16 180.79
[13] c17	$5 \times 8 = 40$	396	16 180.79
majority	$5 \times 11 = 55$	651	22 265.12
majority_5_r1	$5 \times 12 = 60$	737	24 293.23
cm82a_5	$5 \times 15 = 75$	1211	30 377.56
newtag	$8 \times 10 = 80$	651	32 419.82

$w \times h$ Aspect ratio given in hexagonal tiles
SiDBs Number of SiDB quantum dots

A nm^2 Layout area in tiles
Layout area in nm^2

physical constraints as well as a resulting design flow, this section illustrates its application and, thereby, supports the conceptual contributions with reproducible and verifiable data.

The proposed design flow was implemented in C++ and integrated into the open-source FCN framework *fiction* [47]. For logic network representation and optimization, the *mockturtle* [40] library was utilized. Established QCA benchmarks from [13, 43]² were used to generate layouts that are comprehensible by humans for presentation in this work. An excerpt can be found in Table 1 where resulting layout dimensions, the number of needed SiDBs, and area requirements in nm^2 are listed. The generated layouts offer the highest possible throughput of $1/1$ because the applied physical design algorithms ensure the balancing of all signal paths.

As an illustrative example, Figure 6 depicts the synthesized layout of the *par_check* benchmark using the proposed design flow. All obtained design and simulation files as well as the code for their generation are publicly available at [52].

The obtained results demonstrate that the *Bestagon* library and the proposed design automation flow enable automatic layout generation for the promising SiDB platform. In contrast, previous efforts were limited to manual labor and, therefore, restricted to small designs. Furthermore, physical and fabrication restrictions were barely considered in the literature thus far while they are explicitly addressed in this work.

²The *c17* benchmark was originally published in [7].

6 CONCLUSIONS

This work has touched on every foundational aspect for the enablement of SiDB FCN logic design automation: At the physical level, design rules were outlined, which are informed by recent experimental demonstrations, physical models, and realistic fabrication constraints. At the gate level, the *Bestagon* gate library was presented, which provides hexagonal tiles that serve as the basis for physical design and future architectural studies. At the design automation level, a complete design flow was presented that turns logic networks into dot-accurate physical SiDB layouts. Thereby, automatic design for this highly-promising contestant in the FCN domain becomes feasible for the first time.

Since the implementation and all obtained design and simulation files are publicly available [52], this work will serve to facilitate various follow-up studies of interest to the FCN design automation community, including higher-level architectural and application studies into the platform.

There are also opportunities to improve upon the proposed framework. Studies of more intricate clocking floor plans such as *USE* [9] will require the development of intra-super-tile detailed routing capabilities. The advancement of a streamlined operational domain evaluation framework will also be of interest since the existing work is computationally heavy and not trivially quantifiable [30]. Future availability of clocking-informed SiDB logic simulations will also bring us closer to functioning fabricable layouts. This entails that both the *Bestagon* gate library and the proposed software suites will continue to evolve and facilitate the next generation of SiDB FCN design automation research.

ACKNOWLEDGMENTS

The authors would like to express their gratitude towards Amit Patel for the wonderful resources on hexagonal grids on his website *Red Blob Games* and CGP Grey for the title inspiration.

REFERENCES

- [1] R. Achal et al. 2018. Lithography for robust and editable atomic-scale silicon devices and memories. *Nature Communications* 9, 1 (July 2018), 2778.
- [2] N. G. Anderson et al. 2014. *Field-coupled Nanocomputing: Paradigms, Progress, and Perspectives*. Springer, New York.
- [3] A. N. Bahar et al. 2020. Atomic silicon quantum dot: a new designing paradigm of an atomic logic circuit. *TNANO* (2020), 807–810.
- [4] G. H. Bernstein et al. 2005. Magnetic QCA systems. *Microelectronics Journal* 36, 7 (2005), 619–624.
- [5] E. Blair and C. S. Lent. 2018. Clock Topologies for Molecular Quantum-Dot Cellular Automata. *Journal of Low Power Electronics and Applications* 8, 3 (2018).
- [6] E. P. Blair and C. S. Lent. 2003. An Architecture for Molecular Computing using Quantum-Dot Cellular Automata. In *IEEE-NANO*, Vol. 1. IEEE, 402–405.
- [7] F. Brglez and H. Fujiwara. 1985. A Neutral Netlist of 10 Combinational Benchmark Circuits and a Target Translator in Fortran. In *International Symposium on Circuits and Systems (ISCAS)*. IEEE Press, 677–692.
- [8] A. T. Calvino et al. 2022. From Logic to Gates: A Versatile Mapping Approach to Restructure Logic. (2022).
- [9] C. A. T. Campos et al. 2016. USE: A Universal, Scalable, and Efficient Clocking Scheme for QCA. *TCAD* 35, 3 (2016), 513–517.
- [10] H. N. Chiu. 2020. *Simulation and analysis of clocking and control for field-coupled quantum-dot nanostructures*. Master's thesis. University of British Columbia.
- [11] H. N. Chiu et al. 2020. PoisSolver: a tool for modelling silicon dangling bond clocking networks. In *IEEE-NANO*. IEEE, Montreal, QC, Canada, 134–139.
- [12] R. P. Cowburn and M. E. Welland. 2000. Room Temperature Magnetic Quantum Cellular Automata. *Science* 287, 5457 (2000), 1466–1468.
- [13] G. Fontes et al. 2018. Placement and Routing by Overlapping and Merging QCA Gates. In *ISCAS*.
- [14] M. Fuechsle et al. 2012. A single-atom transistor. *Nature Nanotechnology* 7, 4 (April 2012), 242–246.
- [15] M. B. Haider et al. 2009. Controlled Coupling and Occupation of Silicon Atomic Quantum Dots at Room Temperature. *Physical Review Letters* 102, 4 (2009), 046805.
- [16] K. Hennessy and C. S. Lent. 2001. Clocking of Molecular Quantum-dot Cellular Automata. *Journal of Vacuum Science & Technology B* 19, 5 (2001), 1752–1755.
- [17] J. Huang et al. 2005. Tile-based QCA Design Using Majority-like Logic Primitives. *JETC* 1, 3 (2005), 163–185.
- [18] T. Huff et al. 2018. Binary Atomic Silicon Logic. *Nature Electronics* 1 (2018), 636–643. Issue 12.
- [19] T. R. Huff et al. 2017. Atomic white-out: enabling atomic circuitry through mechanically induced bonding of single hydrogen atoms to a silicon surface. *ACS Nano* 11, 9 (Sept. 2017), 8636–8642.
- [20] J. Jiao et al. 2003. Building Blocks for the Molecular Expression of Quantum Cellular Automata. Isolation and Characterization of a Covalently Bonded Square Array of Two Ferrocenium and Two Ferrocene Complexes. *Journal of the American Chemical Society* 125, 25 (2003), 7522–7523.
- [21] R. W. Keyes et al. 1970. Minimal Energy Dissipation in Logic. *IBM Journal of Research and Development* 14, 2 (1970), 152–157.
- [22] R. Landauer. 1961. Irreversibility and Heat Generation in the Computing Process. *IBM Journal of Research and Development* 5, 3 (1961), 183–191.
- [23] C. S. Lent et al. 1993. Quantum Cellular Automata. *Nanotechnology* 4, 1 (1993), 49.
- [24] C. S. Lent et al. 2003. Molecular Quantum-Dot Cellular Automata. *Journal of the American Chemical Society* 125, 4 (2003), 1056–1063.
- [25] C. S. Lent et al. 2006. Bennett clocking of quantum-dot cellular automata and the limits to binary logic scaling. *Nanotechnology* 17, 16 (2006), 4240–4251.
- [26] C. S. Lent and P. D. Tougaw. 1997. A device architecture for computing with quantum dots. *Proc. IEEE* 85, 4 (April 1997), 541–557.
- [27] L. Livadaru et al. 2010. Dangling-bond charge qubit on a silicon surface. *New Journal of Physics* 12, 8 (Aug. 2010), 083018.
- [28] R. Lupoiu et al. 2022. Automated Atomic Silicon Quantum Dot Circuit Design via Deep Reinforcement Learning. arXiv:2204.06288
- [29] S. S. H. Ng. 2020. *Computer-aided design of atomic silicon quantum dots and computational applications*. Master's thesis. University of British Columbia.
- [30] S. S. H. Ng et al. 2020. SIQAD: A Design and Simulation Tool for Atomic Silicon Quantum Dot Circuits. *TNANO* 19 (2020), 137–146.
- [31] N. Pavlíček et al. 2017. Tip-induced passivation of dangling bonds on hydrogenated Si(100)-2×1. *Applied Physics Letters* 111, 5 (2017), 053104.
- [32] J. L. Pitters et al. 2011. Charge control of surface dangling bonds using nanoscale Schottky contacts. *ACS Nano* 5, 3 (March 2011), 1984–1989.
- [33] H. Qi et al. 2003. Molecular Quantum Cellular Automata Cells. Electric Field Driven Switching of a Silicon Surface Bound Array of Vertically Oriented Two-Dot Molecular Quantum Cellular Automata. *Journal of the American Chemical Society* 125, 49 (2003), 15250–15259.
- [34] M. Rashidi et al. 2016. Time-resolved single dopant charge dynamics in silicon. *Nature Communications* 7, 1 (Dec. 2016), 13258.
- [35] M. Rashidi et al. 2018. Initiating and monitoring the evolution of single electrons within atom-defined structures. *Physical Review Letters* 121, 16 (Oct. 2018), 166801.
- [36] D. A. Reis et al. 2016. A methodology for standard cell design for QCA. In *ISCAS*. 2114–2117.
- [37] J. Retallick et al. 2021. Low-Energy Eigenspectrum Decomposition (LEED) of Quantum-Dot Cellular Automata Networks. *TNANO* 20 (2021), 104–112.
- [38] H. Riener et al. 2019. On-the-fly and DAG-aware: Rewriting Boolean Networks with Exact Synthesis. In *DATE*. 1649–1654.
- [39] C. G. Smith et al. 2003. Realization of quantum-dot cellular automata using semiconductor quantum dots. *Superlattices and Microstructures* 34, 3-6 (2003), 195–203.
- [40] M. Soeken et al. 2019. The EPFL Logic Synthesis Libraries. arXiv:1805.05121v2
- [41] J. Timler et al. 2002. Power Gain and Dissipation in Quantum-dot Cellular Automata. *Journal of Applied Physics* 91, 2 (2002), 823–831.
- [42] G. Toth et al. 1999. Quasiadiabatic switching for metal-island quantum-dot cellular automata. *Journal of Applied Physics* 85, 5 (1999), 2977–2984.
- [43] A. Trindade et al. 2016. A Placement and Routing Algorithm for Quantum-dot Cellular Automata. In *SBCCI*.
- [44] V. Vankamamidi et al. 2006. Clocking and Cell Placement for QCA. In *IEEE-NANO*, Vol. 1. IEEE, 343–346.
- [45] M. D. Vieira et al. 2021. Novel three-input gates for silicon quantum dot. In *SBCCI*. 1–6.
- [46] M. Walter et al. 2018. An Exact Method for Design Exploration of Quantum-dot Cellular Automata. In *DATE*. 503–508.
- [47] M. Walter et al. 2019. fiction: An Open Source Framework for the Design of Field-coupled Nanocomputing Circuits. arXiv:1905.02477
- [48] M. Walter et al. 2019. Placement & Routing for Tile-based Field-coupled Nanocomputing Circuits is \mathcal{NP} -complete. *JETC* 15, 3 (2019).
- [49] M. Walter et al. 2019. Scalable Design for Field-coupled Nanocomputing Circuits. In *ASP-DAC*. ACM New York, NY, USA, 197–202.
- [50] M. Walter et al. 2020. Verification for Field-coupled Nanocomputing Circuits. In *DAC*.
- [51] M. Walter et al. 2021. One-pass Synthesis for Field-coupled Nanocomputing Technologies. In *ASP-DAC*. ACM New York, NY, USA, 574–580.
- [52] M. Walter, S. S. H. Ng, K. Walus, and R. Wille. 2022. Bestagon Gate Library Repository – Supplementary Data. <https://github.com/cda-tum/sidb-bestagon-gate-library>.
- [53] R. A. Wolkow et al. 2014. *Silicon Atomic Quantum Dots Enable Beyond-CMOS Electronics*. Springer, 33–58.
- [54] S.Y. Wu et al. 2016. A 7nm CMOS platform technology featuring 4th generation FinFET transistors with a 0.027um² high density 6-T SRAM cell for mobile SoC applications. In *IEDM*. 2.6.1–2.6.4.